

Chapter 10

Topologically Complex Morphologies in Block Copolymer Melts



J. J. K. Kirkensgaard

10.1 Introduction

1 Polymers are macromolecules built from chains of subunits. Naturally occurring
 2 examples of polymers include DNA and proteins built from chains of nucleic and
 3 amino acids respectively or cellulose built from chains of connected glucose units.
 4 Most synthetic polymers are built from a single subunit, the monomer, and are termed
 5 homopolymers. The connection of two or more homopolymer chains into a larger
 6 macromolecule is termed a *block copolymer* and these can be made with multiple
 7 components connected into both linear or branched molecular architectures as illus-
 8 trated in Fig. 10.1. Block copolymers remain a subject of significant research interest
 9 owing to the control and reproducibility of physical properties and the many fasci-
 10 nating nanoscale structures which can be obtained [1]. The self-assembly behavior
 11 of block copolymers originate from the tendency of the various polymer chains to
 12 undergo phase separation which is however inherently constrained due to the molec-
 13 ular connectivity. This leads to the formation of ordered mesostructures with char-
 14 acteristic length scales on the order of the chain sizes, typically tens of nanometers.
 15 The formation of ordered structures in block copolymer systems stems from a com-
 16 petition between two effects: the entropic penalty associated with chain stretching
 17 and compression causing a preference for domains with constant thickness, and an
 18 enthalpic penalty associated with interfacial energy causing a preference for domain
 19 shapes which minimise surface area. In equilibrium a compromise between these
 20 factors is achieved by forming interfacial surfaces which tend to have approximately
 21 constant mean curvature. The nanostructures described below represent a tremen-
 22 dous potential for future technological applications because they provide a bottom-up
 23 route to materials with tailored optical, mechanical, electrical and photovoltaic prop-

J. J. K. Kirkensgaard (✉)

Niels Bohr Institute, University of Copenhagen, Copenhagen, Denmark
 e-mail: jjkk@nbi.dk

© Springer International Publishing AG 2018
 S. Gupta and A. Saxena (eds.), *The Role of Topology in Materials*,
 Springer Series in Solid-State Sciences 189,
https://doi.org/10.1007/978-3-319-76596-9_10

1

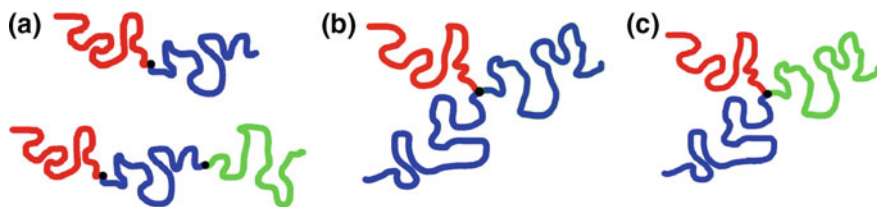


Fig. 10.1 Block copolymers. Covalent bonding of different polymer chains A, B, C, ... results in block copolymers of varying molecular architecture, here **a** linear AB diblock copolymers and ABC triblock terpolymers, **b** star-shaped AB₂ miktoarm copolymer and **c** ABC star miktoarm terpolymer

.. please add a period at end of caption - applies to ALL figures!

24 erties (and combinations thereof), for example through phase selective chemistries
 25 or selective sequential removal of the blocks.

26 In this chapter two notions of topology will be relevant: First we will talk about
 27 the topology of the macromolecules, i.e. the arrangement of chains in the individual
 28 copolymers, but we will use the term 'molecular architecture' to describe this. We
 29 will focus in detail on the molecular architecture as a topological variable and how
 30 it influences the morphologies one finds in self-assembled block copolymer systems.
 31 Secondly, we present a range of examples of morphologies with different and
 32 sometimes very complex mesoscale topology, i.e. patterns which emerges from the
 33 tendency of these molecules to undergo spatial phase separation under the constraint
 34 of the molecular connectivity and which show periodicities on the length scale of
 35 the chain sizes as described above. We will restrict ourselves to looking at polymer
 36 *melts*, i.e. polymers in a liquid state above the glass transition temperature without
 37 any added solvent.

38 10.2 AB Block Copolymers

39 The simplest block copolymers are AB diblocks where two polymer chains A and
 40 B are connected at a single junction point (see Fig. 10.1a). Diblock copolymers have
 41 been studied for decades and their self-assembly are generally well understood [3].
 42 The structural phase behaviour of AB diblock copolymers is usually described as a
 43 function of two parameters: the composition, i.e. the relative volume fractions of the
 44 two components, and the degree of segregation described by the product χN where χ
 45 is the Flory-Huggins interaction parameter describing the chemical incompatibility
 46 between the different chains and N is the degree of polymerisation (the length of
 47 the polymer) [4, 5]. A characteristic feature of diblock copolymer self-assembly is
 48 that for increasing segregation, the phase behaviour becomes dominated by the com-
 49 position. As a function of the composition described by the A component volume
 50 fraction $f = f_A$ ($f_B = 1 - f_A$) the universal phase diagram in the strong segregation
 51 limit consists of four ordered morphologies namely lamellar, bicontinuous double

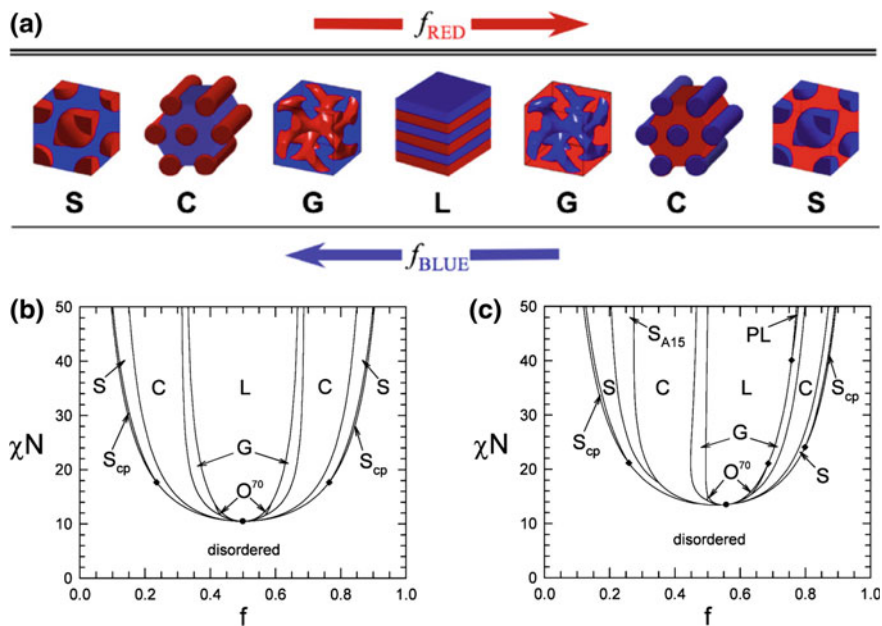


Fig. 10.2 Phase diagrams of AB-type block copolymers. **a** Morphologies found in AB diblock systems. S: cubic sphere packing, C: hexagonal cylinders, G: bicontinuous double gyroid, L: Lamellar. Figure from [2]. **b** Theoretical phase diagram for AB diblock copolymers. The O^{70} phase is an orthorhombic network phase described below. **c** Theoretical phase diagram for branched AB_2 miktoarm star copolymer. Phase diagrams from [3]

52 gyroid, hexagonally arranged cylinders and a cubic bcc sphere packing, all in principle
 53 appearing symmetrically around a 50/50 composition ($f = 0.5$). These phases
 54 are illustrated in Fig. 10.2a and a complete phase diagram based on a self-consistent
 55 field theory prediction is shown in Fig. 10.2b. The χ parameter for a given polymer
 56 pair is usually temperature dependent so that one can decrease the segregation by
 57 raising the temperature (and vice versa). This means that at $f = 0.4$ for example one
 58 should in principle be able to find phase transitions from $L \rightarrow G \rightarrow C \rightarrow$ disorder by
 59 increasing temperature (thus moving vertically in the phase diagram).¹ The latter is
 60 termed the order-disorder transition and the others order-order transitions. Inspection
 61 of the morphologies in Fig. 10.2a reveal that these phases are either based on simple
 62 topologies like planes, cylinders, spheres or in the case of the double gyroid, the

¹There are a number of practical subtleties associated with this statement. First of all it requires that the molecular weight (or N) is not so large that the temperatures required to reach the transitions disintegrates the molecules, and second, the temperature range has to be above the glass transition temperature T_g which is a property of the specific chains. We will assume we are in a region of size and temperature where the notion of phase transitions makes sense. Note however that in structural studies of block copolymer morphologies one often utilises the glass transition of one or more of the chains to effectively 'freeze' a given structure by a rapid temperature quench.

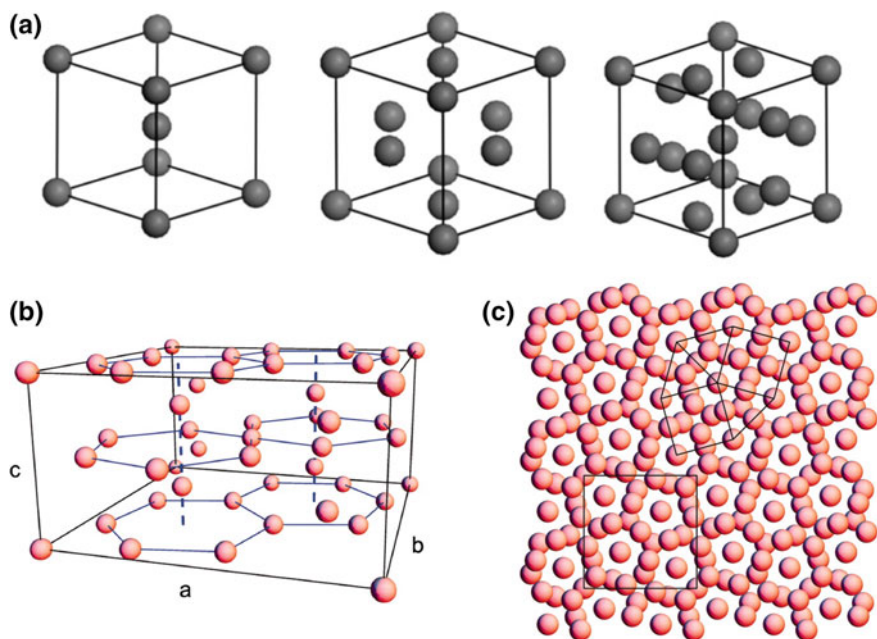


Fig. 10.3 Sphere packings found in block copolymer systems. **a** Cubic packings BCC, FCC and A15. Figure from [7]. **b** Frank–Kasper σ -phase. Figure from [8]

Should be b,c Frank-Kasper etc.

63 more complex topology of networks whose midsurface is describable as a minimal
 64 surface [6]. Whichever it is, an order-order transition often necessitates a change of
 65 topology. Here we will not discuss such phase transitions in detail, but will rather
 66 focus on the effect of changing the molecular architecture and composition.

67 In Fig. 10.2c a phase diagram of two-component AB_2 miktoarm stars are shown.
 68 For a given composition quantified by f , the change in molecular architecture induces
 69 increased interfacial curvature leading to shifts in the phase diagram, increasing
 70 for example the regions of spherical packings by introducing the A15 phase (see
 71 Fig. 10.3) and also stabilising another new morphology, the perforated lamellae (PL)
 72 where lamellar sheets of the B-component is protruded by hexagonally arranged
 73 pillars of the majority matrix component A. Also, the O^{70} network phase exhibits
 74 a larger region on the $f > 0.5$ side of the diagram with the B-component forming
 75 the network and the A-component the matrix [3]. As we shall see below, chang-
 76 ing the molecular architecture allows the formation of spectacular structures when
 77 increasing the number of components to more than two. The formation of low sym-
 78 metry sphere packings is an ongoing topic in soft matter self-assembly [9] with a
 79 prominent example found in a block copolymer melt, namely the discovery of a large
 80 unit cell tetragonal structure known from metal alloys as the σ Frank–Kasper phase
 81 [8], see Fig. 10.3b, c. The low symmetry sphere packings like A15 and the σ phase
 82 are known as approximants to aperiodic quasicrystalline arrangements characterised

83 by rotational symmetry, but not translational symmetry. The finding of the σ phase
84 recently led to the discovery of a long-lived metastable dodecagonal quasicrystalline
85 phase in a block copolymer system [10].

86 10.3 ABC Block Copolymers

87 The addition of a third component dramatically increases the morphological phase
88 space as seen with linear ABC terpolymers where a large number of different structures
89 have been found [1, 11]. A unifying feature between the structures formed in
90 linear ABC systems and those found in simpler AB systems is that they are all char-
91 acterised by the *interfaces* of each pair of polymer species. So speaking in terms of
92 structural motifs, linear ABC block copolymers also explore variations of the surface
93 topologies mentioned above: sphere, cylinder, plane, networks/minimal surface, but
94 in multicolor versions, see Fig. 10.4 for a few examples. Nevertheless, the addition of
95 a third component still allows more detailed control of the resulting morphologies and
96 also opens up regions in the phase diagram of new and complex phases. An example
97 is the poly(isoprene-*b*-styrene-*b*-ethylene oxide) linear triblock terpolymer system
98 (ISO) studied experimentally and theoretically by Bates and colleagues [12] where
99 several complex network phases are shown to form in the phase region between 2-
100 and 3-colored lamellar structures, see Fig. 10.4b, c. The orthorhombic O^{70} phase is a
101 single net structure while the Q^{230} and Q^{214} phases are both of the double gyroid type.
102 The difference is the molecular packing: in the Q^{230} the nets are symmetric while in
103 Q^{214} the two nets are built from different chemical species lowering the symmetry to
104 the chiral subgroup since each of the double gyroid nets are chiral enantiomers (of
105 opposite handedness). The formation of network phases like the double gyroid is a
106 well-known phenomena in soft matter self-assembly where it is found ubiquitously
107 in for example lipid and surfactant systems forming lyotropic liquid crystals [6]. Here
108 the 3-connected double gyroid appears as one of typically three phases formed, the
109 others being the 4-connected double diamond phase and the 6-connected primitive
110 phase - all of cubic symmetry. In pure AB and ABC linear block copolymer melts all
111 network phases found is of the 3-connected kind which is ultimately a result of the
112 configurational entropy loss associated with chain stretching which is not penalised
113 in surfactant type systems: The chain stretching required in polymer systems to fill
114 network nodes with more than 3 connectors becomes prohibitive for the formation
115 of those phases unless alleviated by the addition of shorter homopolymers chains
116 or some kind of nanoparticle which can reside in the nodal centers as space fillers
117 [13, 14].

118 However, as illustrated above with the AB_2 miktoarm stars a change in molecular
119 architecture can induce increased interfacial curvature and stabilise new phases.
120 In Fig. 10.5 a simulated phase diagram is shown of $A(BC)_2$ miktoarm star melts.
121 A reference structure where each chain is roughly the same length assembles to a
122 perforated lamellae structure (verified experimentally in [15]) and as each arm length
123 is varied relative to that a number of new structures appear on the periphery of the

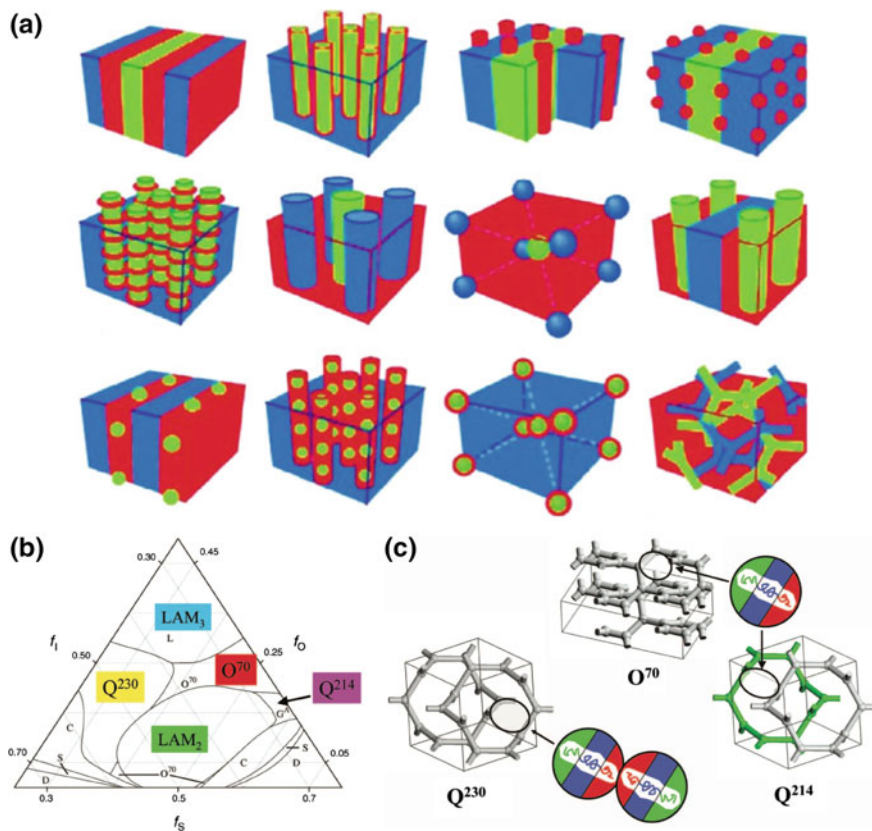


Fig. 10.4 Linear ABC triblock copolymer phases. **a** A selection of structures formed in linear ABC systems. Figure from [11]. **b** Theoretical ternary phase diagram showing the appearance of three different 3-connected network phases [12], the orthorhombic O^{70} phase and the two cubic double gyroid phases Q^{230} and Q^{214} . **c** Network representations and local molecular configurations of the networks from **b**. Figures (b, c) from [12]

124 perforated lamellae region. First, as the A arm is shortened, a single gyroid phase
 125 emerges (GL_{AB}) - note that this is a chiral structure - while for longer A arms a double
 126 diamond phase is stabilised. Increasing the middle B-block leads to a hybrid structure
 127 with the red A component forming a spherical packing while the green C species
 128 forms a 3-connected gyroid-like network. Note that because of the multicomponent
 129 nature of the molecules, the middle B blocks in these phases form topologically very
 130 complex continuous morphologies with channels and cavities.

131 As mentioned above, a unifying feature between the structures formed in the
 132 linear AB and ABC systems shown in Fig. 10.1 is that they are all characterised by the
 133 interfaces of each pair of polymer species. Although the $A(BC)_2$ miktoarm stars allow
 134 the formation of a range of topologically complex phases, they can still effectively
 135 be thought of as a linear ABC molecule only with added splay due to the two diblock

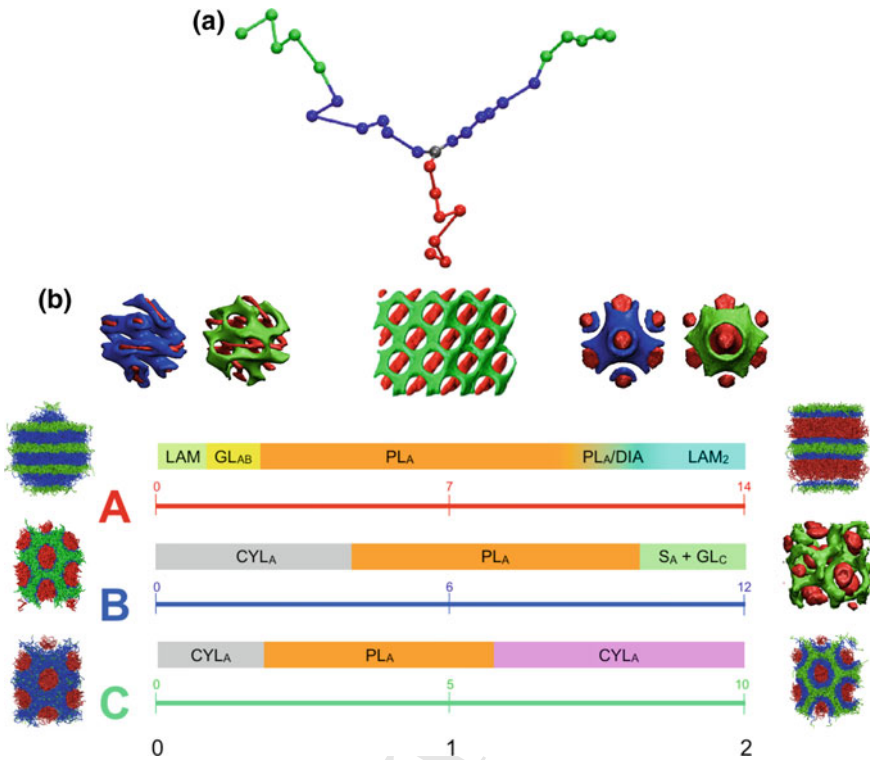


Fig. 10.5 **a** $A(BC)_2$ miktoarm star. **b** Simulated phase diagram of $A(BC)_2$ miktoarm stars from [16]

136 chains. This is because the topology of the star branch point only involves two of the
 137 chain species and so effectively acts in the same way as the connection of a linear
 138 molecule. However, another option when adding a third component is to make a star-
 139 like topology where all species meet at the branch point. Such molecules are called
 140 ABC miktoarm star terpolymers (Fig. 10.1). The self-assembly behaviour of ABC
 141 stars have been investigated experimentally [17] and theoretically [5–8]. The generic
 142 theoretical phase diagram as described by these sources is shown in Fig. 10.6 under
 143 the compositional constraint of two components occupying equal volume fractions
 144 and of symmetric interaction parameters between the different polymer species.
 145 Compared with the self-assembly of linear block copolymers a fundamental result
 146 appears despite these severe constraints: dictated by the molecular star topology ABC
 147 lines are formed where the three different interfaces between AB, AC and BC meet
 148 [18–21]. As a consequence, a sequence of columnar structures with cross-sections
 149 following various polygonal tiling patterns appears. This sequence of tilings has been
 150 predicted from all the earlier mentioned theoretical studies and has been found in a
 151 number of experimental ABC 3-miktoarm star terpolymer systems [17].

Yes this is wrong, sorry.
 Should be [18,21-23]
 ex cite code if you need it is
 cite(Dotera:2002, jkk, tiling,
 Huang,08, jkk, physreve)

[AQ2]

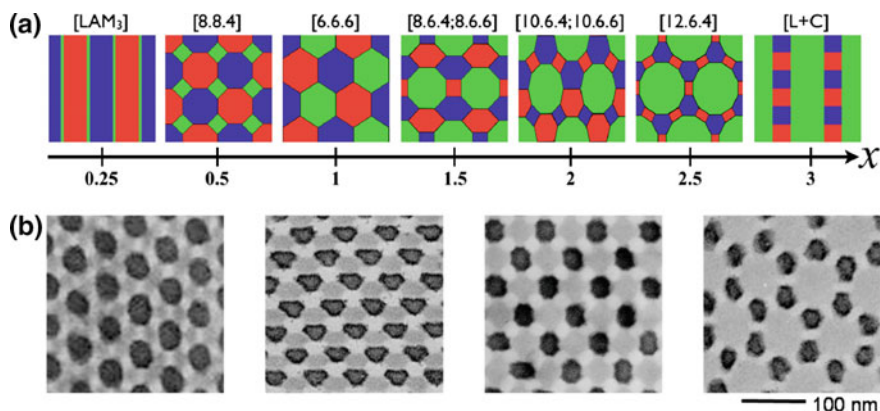


Fig. 10.6 **a** Generic phase diagram for ABC 3-miktoarm star terpolymers. The A and B components are constrained to occupy equal volume fractions and interactions between all unlike components are symmetric [18, 21–23]. The different phases are placed at their approximate compositional positions quantified by the parameter x , the volume ratio of the C and A (= B) components. The tilings are denoted by their Schläfli symbol [18, 21], a set of numbers $[k_1.k_2.\dots.k_l]$ indicating that a vertex is surrounded by a k_1 -gon, a k_2 -gon, ... in cyclic order. Tilings with more than one topologically distinct vertex are named as $[k_1.k_2.k_3; k_4.k_5.k_6]$. Color code: A: red, B: blue, C: green. **b** Examples of tiling patterns from poly(isoprene-*b*-styrene-*b*-2-vinylpyridine) miktoarm star terpolymers visualized by transmission electron microscopy. Images from [17]

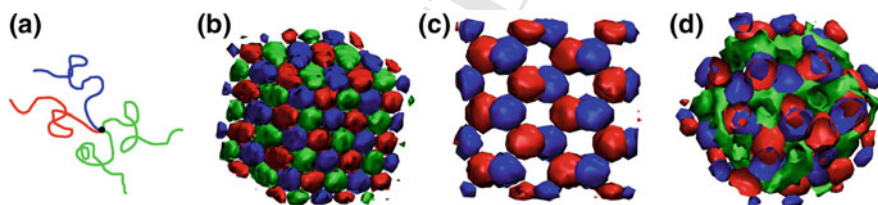


Fig. 10.7 Varying the composition by adding chains of equal length instead of increasing the length of one chain results in completely new structures [23]. **a** An ABC_2 star ($x = 2$). **b** For $x = 1$ the result is still the [6.6.6] tiling. **c** For $x = 2$ a double diamond network structure is found with one net built from alternating A and B domains. **d** For $x = 3$ the system also forms a striped network structure but now with the topology of the double gyroid structure with one net built from alternating red and blue domains. Figures from [23]

152 Again, one can influence the interfacial curvature by altering the molecular archi-
 153 tecture. In Fig. 10.7 the composition of ABC stars is altered by adding chains of equal
 154 length instead of increasing the length of one chain. Direct comparison with the ABC
 155 star phase diagram in Fig. 10.6 shows that the tiling patterns at $x = 2$ and $x = 3$ are
 156 now replaced with new decorations of the bicontinuous motifs of the diamond and
 157 gyroid network patterns. In these new structures one of the two nets are now built
 158 from alternating globular domains of the minority components. The striped double
 159 diamond has been found experimentally in a blend system as described below [24].

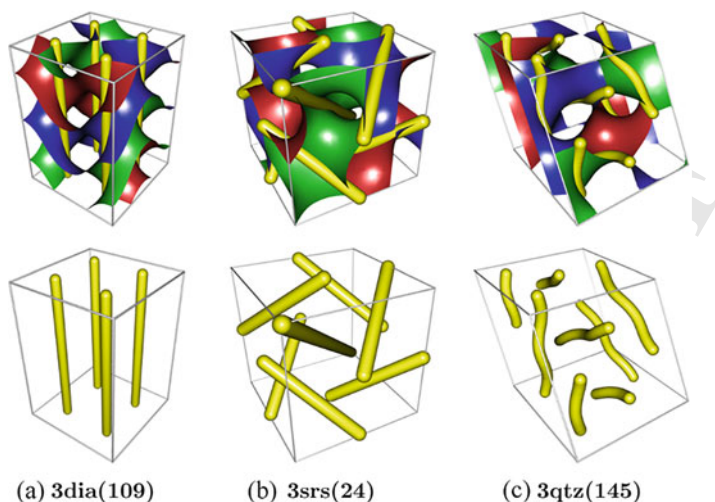


Fig. 10.8 Examples of tricontinuous candidate patterns topologically consistent with the star molecular architecture [20]. Yellow lines indicate the triple lines along which the star molecular cores pack. **a** 3 intertwined diamond nets. **b** 3 intertwined gyroidal srs-nets (all of same handedness, so a chiral structure). **c** 3 intertwined quartz qtz-nets (also chiral). Figure from [28]

160 As mentioned above, the connectivity of ABC stars sets a topological constraint
 161 on the possible self-assembly morphologies but also leads to new possibilities. One
 162 very exciting option set forth by Hyde and co-workers is the formation of new tri- and
 163 polycontinuous patterns [20, 25]. They showed that such patterns were **topological** topologically ?
 164 consistent with the star molecular architecture and hypothesised their formation in
 165 star systems. A number of candidate structures were suggested (see Fig. 10.8) and
 166 evaluated in terms of energetics but any of them remains to be found experimentally in
 167 an ABC star system.² However, by suitably adjusting the molecular architecture and
 168 chemistry of ABC stars it turns out one can favour a thermodynamically stable tricon-
 169 tinuous structure based on three intertwined so-called ths-nets as was demonstrated
 170 using self-consistent field theory in [28] (see Fig. 10.9). This is a spectacular network
 171 structure effectively carving up space into three separated congruent labyrinths, each
 172 with a separate chemistry and thus properties. The key to stabilising this structure
 173 stems from the introduction of an extended core which effectively alters the balance
 174 between entropic and enthalpic free energy contributions, ultimately allowing this
 175 new pattern to outfavour the prismatic hexagonal honeycomb.

²One of the predicted tricontinuous patterns have in fact been identified in both a hard and a soft matter context. In [26] such a pattern was found in a mesoporous silica and the same structure was later identified in a lyotropic liquid crystalline surfactant system [27]. However, in those cases the channels all contain the same material unlike the structures described here which have a different chemical species inside each channel.

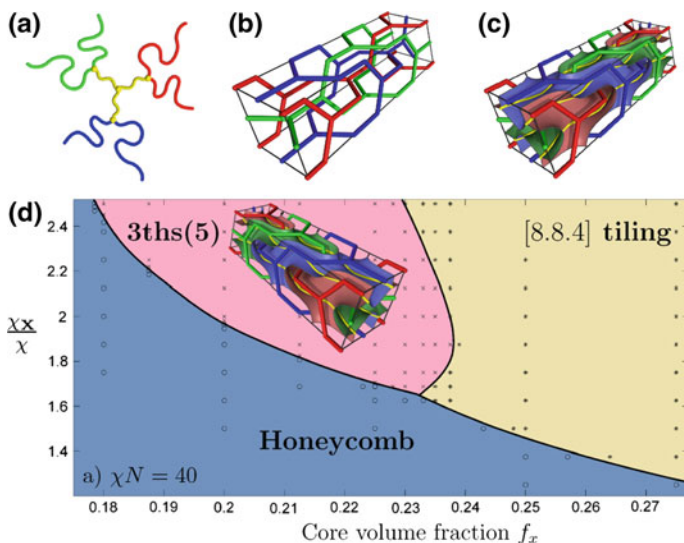


Fig. 10.9 **a** A dual chain core ABC star triblock copolymer. **b** Triply intergrown *ths*-nets. **c** As in **b** but showing the interfaces also. **d** Phase diagram from [28]: As a function of the core volume fraction and the interaction strength three structures dominate the phase diagram, one of which is a spectacular tricontinuous network structure

10.4 Blending Molecular Architectures

176

177 Blending polymers has been a heavily used strategy for many years to obtain a material with new properties akin to alloys in metallurgy. This also applies to block copolymers where one approach is to swell a particular domain with shorter homopolymer chains of the same species - in analogy to swelling in lyotropic liquid crystalline systems. For example, blending an ABC star which alone forms the [6.6.6] tiling pattern with C homopolymer chains can lead to a zinc-blende structure with alternating AB domains building up a diamond network [24] as the one illustrated in Fig. 10.7c above. If the swelling agent is not a homopolymer chain but another block copolymer, compatibility between pairs of blocks of both molecules becomes another control parameter for structure formation. An example is shown in Fig. 10.10 where blending an ABC star which forms the [12.6.4] tiling alone with AB diblock copolymers causes the A and B components to swap polygonal symmetry positions in the tiling pattern [29]. Thus, blending opens up the possibility of fine-tuning the structures found in the pure systems or allowing completely new patterns to appear. However, the possible phase space of a blend of different block copolymers stars is enormous. The main variables in play are (i) the molecular topology, i.e. the connectivity of the chains, (ii) the composition, i.e. the volume fractions of the different chains including the blend ratio, (iii) the chemical nature of the different polymer species, i.e.

194

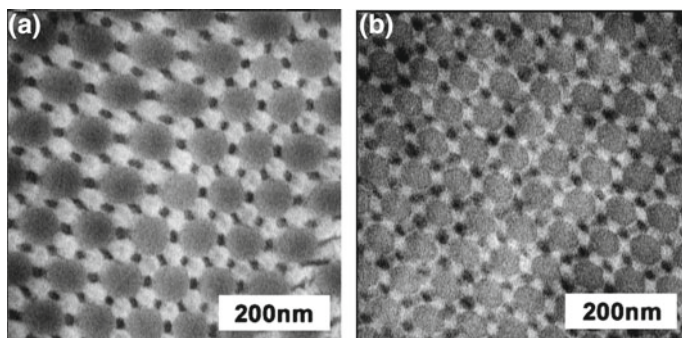


Fig. 10.10 Blending block copolymers. **a** An asymmetric polystyrene-*b*-polybutadiene-*b*-poly(2-vinylpyridine) ($S_{34}B_{11}V_{55}$) miktoarm star terpolymer forms a [12.6.4] tiling on its own (subscripts indicate molecular weight). The minority B component forms the dark 4-sided domains while the S component forms the white hexagonal domains in the tiling. **b** When blended with a $S_{45}V_{55}$ diblock copolymer the tiling pattern remains [12.6.4] but the chemical nature of the hexagons and squares swap so that B now forms hexagons and S forms squares. Figures from [29]

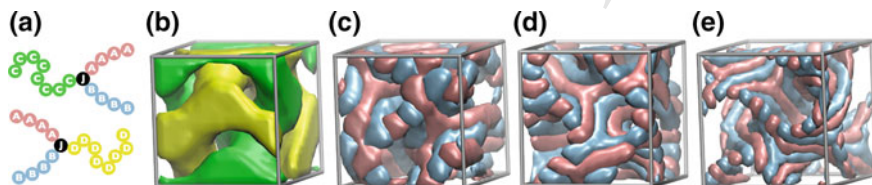


Fig. 10.11 **a** Blending ABC and ABD 3-miktoarm star terpolymers. All molecules contain equal sized A (red) and B (blue) arms, and longer C (green) and D (yellow) arms, but also of equal size. The parameter x (equal to $8/4 = 2$ in this image), corresponds to the number ratio of C to A beads. **b** C and D domain geometry, a pair of intertwined gyroid nets. **c–g** Single unit cell snapshots illustrating the curved striped pattern formed by the minority components A and B for varying x . **c** $x = 2$, **d** $x = 3.67$, **e** $x = 6$. Note the 3-fold branching for all values of x . Figures from [30]

195 their mutual interaction parameters. Secondary variables can be polydispersity of
196 the chains and chain flexibility for example [1].

197 In Fig. 10.11 an example is shown where a series of spectacular structures are
198 predicted to form in blends of two different miktoarm stars [30]. Blending ABC
199 and ABD star triblocks in a 50/50 ratio and with the majority domains (green C +
200 yellow D) 2–7 times longer than the minority components (red A + blue B) a series
201 of complex chiral network structures are predicted to form. The C and D species
202 form two chiral enantiomeric nets separated by a membrane following the gyroid
203 surface. As the C and D chains grow, the overall structure remains a chiral gyroid, but
204 unlike all hitherto found gyroid(-like) structures, the channels in these new structures
205 constitute majority domains resulting in the formation of a thin hyperbolic film. AQ3

206 Depending on the composition, interactions and molecular architectures in play,
207 the minority components form remarkable structures on this hyperbolic curved film,
208 in particular ordered branched structures which can be thought of as ‘hyperbolic

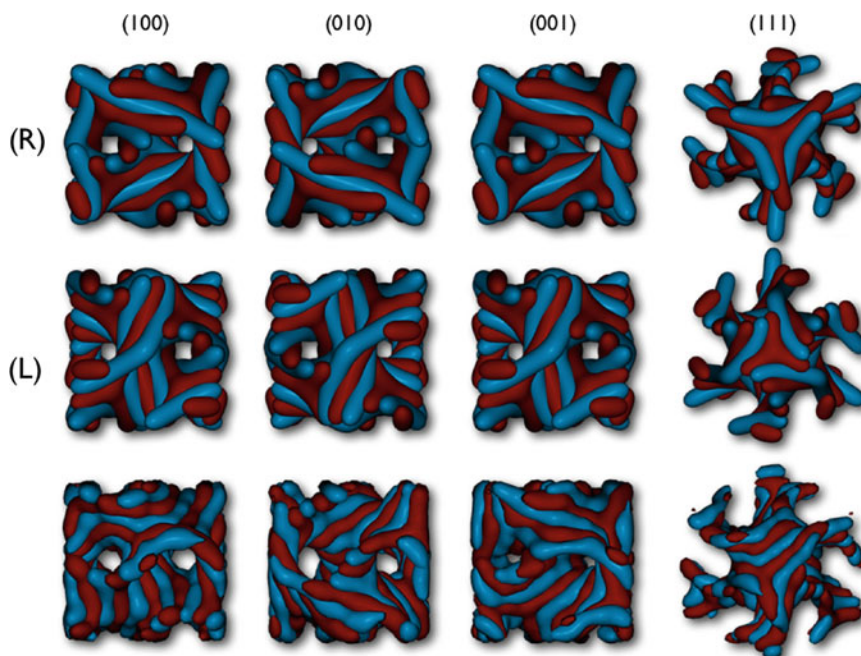


Fig. 10.12 Comparison of ideal left- (L) and right-handed (R) patterns (top and middle rows) viewed from various directions with a self-assembled morphology formed in a simulated mixture of terpolymers with $x = 4$ (bottom row). The simulated morphologies can be seen to match both of the ideal left- and right-handed patterns in distinct patches of the unit cell and are therefore of mixed chirality

209 lamellae'. It is important to realise that if the film was flat, regular lamellae would
 210 form, but because of the curvature of the film branching has to occur. Remarkably,
 211 it turns out that these branched patterns are theoretically related to a family of
 212 tilings in the hyperbolic plane which when embedded on the gyroid surface yields
 213 distinct interwoven chiral nets, always of the same handedness and which changes
 214 topology systematically as a function of composition. The non-chiral nature of the
 215 block copolymer preclude a preferred handedness, which in the numerical simulations
 216 results in domains of opposite chirality forming, ultimately giving rise to defects, see Fig. 10.12. Nevertheless, the ideal mesostructures of these patterns in
 217 three-dimensional space are spectacular and extraordinarily complex. The minority
 218 components form multiple threaded chiral nets (all of equal handedness) whose
 219 topologies are that of the gyroid net. The number of disjoint nets making up the
 220 hyperbolic film can be up to 54 [30]. These intricate self-assemblies of liquid-like
 221 domains thus rival the complex interwoven networks found in synthetic metal-organic
 222 frameworks [31].
 223

224 **10.5 Concluding Remarks**

225 The role of molecular architecture (chain topology) has been shown to be a defining
 226 variable influencing the resulting self-assembly morphologies in block copolymer
 227 melts and a number of patterns with complex topology has been presented from
 228 experiments and simulations. From a topological perspective perhaps the simplest
 229 way to condense the message presented here is shown in Fig. 10.13. Here symmetric

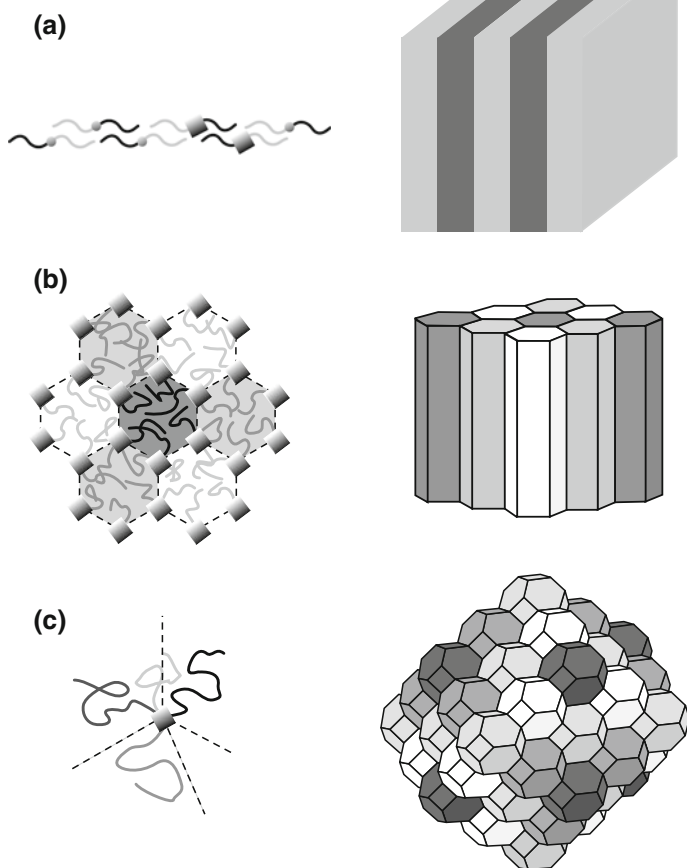


Fig. 10.13 The mutual interfacial dimensionality changes with the molecular architecture for symmetric block copolymers. **a** Diblocks form lamellae with 2D (surface) interfaces. **b** ABC star triblocks form tiling patterns with 2D and 1D (line) interfaces. **c** ABCD star tetrablocks form cellular packings with 2D, 1D and 0D (point) interfaces. This particular cellular packing is a 4-colored Kelvin foam, i.e. each component forms a closed cell in the shape of a truncated octahedron surrounded by 14 neighbors. This structure has been predicted to form in symmetric ABCD stars [32]. Figure from [32]

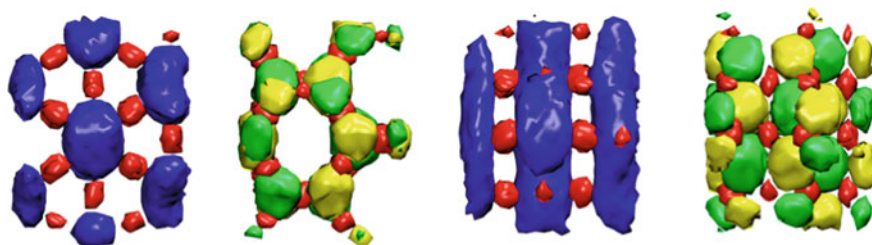


Fig. 10.14 Edge-on (left) and top-down (right) split views of morphology formed in an asymmetric four-armed ABCD miktoarm star with arm length ratios of 1:4:2:2. Color code: A (red), B (blue), C (green), D: (yellow)

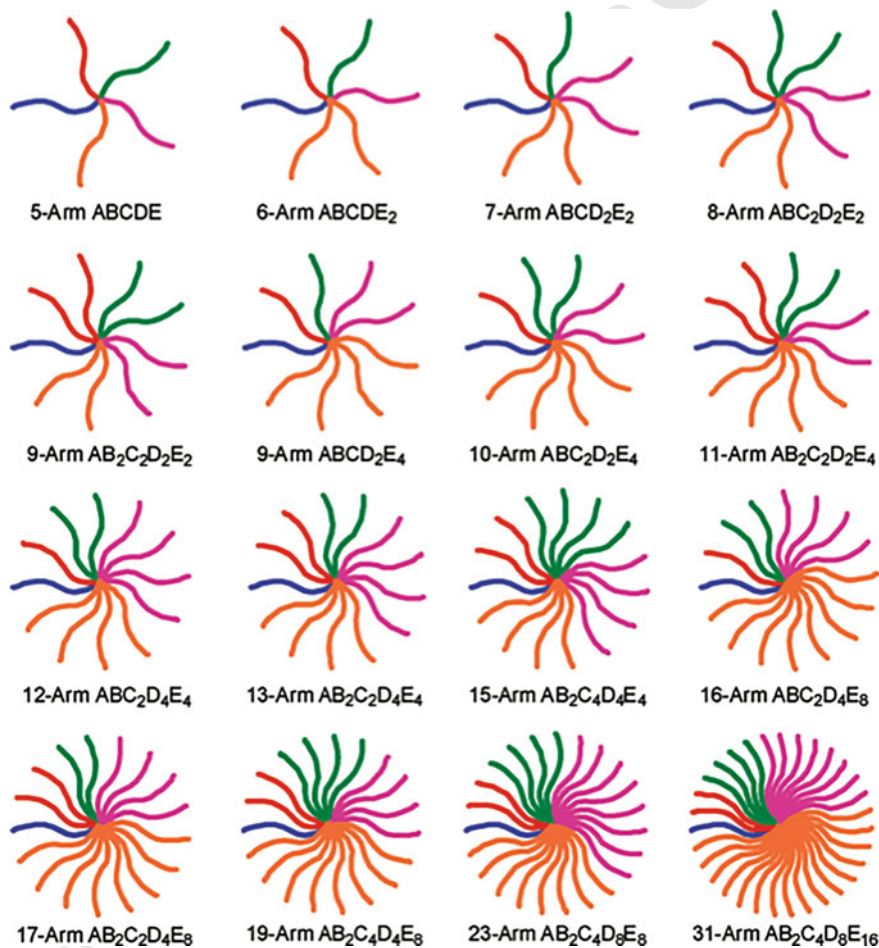


Fig. 10.15 A selection of possible structures of asymmetric star polymers obtained by Hirao and co-workers using advanced iterative synthetic techniques. Figure from [33]

230 AB diblocks are compared as a 2-star with an ABC 3-star and a ABCD 4-star and it is
231 clear that the interfacial dimensionality changes as the molecular topology is altered.
232 Each pair of species defines a surface and as the surfaces have to meet in space we
233 go from 2D interfaces to 1D line interfaces and finally to 0D point interfaces in a
234 cellular packing. In the latter case, Monte Carlo simulations of symmetric ABCD 4-
235 miktoarm stars by Dotera [32] showed that a 4-colored Kelvin foam was the optimal
236 packing, and not for example a square 4-colored tiling pattern.

237 As the molecular composition is altered away from the symmetric case, the
238 resulting structural response becomes a combination of these motifs as illustrated in
239 Fig. 10.14. Here an asymmetric ABCD star is shown to form a hexagonal columnar
240 structure with elements of a [12.6.4] tiling along the cylinder axis, but apart from the
241 cylinders themselves remains a cellular structure. Many more structures are expected
242 to be found in these and higher order block copolymer molecules as combinations
243 of the topologies displayed here. From a theoretical perspective we can continue
244 to add chains but the synthetic community is in some sense way ahead of theory:
245 In Fig. 10.15 a range of examples are shown of incredible molecular architectures
246 synthesised in the group of A. Hirao. The potential morphologies and topologies to
247 be found in these systems is unknown as these molecules are still largely unexplored
248 structurally both theoretically and experimentally.

249 **Acknowledgements** The author wishes to gratefully acknowledge colleagues and mutual co-
250 authors of the authors own research presented in this chapter, in particular Stephen T. Hyde, Liliana
251 de Campo, Myfanwy Evans, Martin C. Pedersen, Gerd E. Schröder-Turk, Michael G. Fischer,
252 Panagiota Fragouli, Nikos Hadjichristidis and Kell Mortensen.

253 References

- 254 1. F. Bates, M. Hillmyer, T. Lodge, C. Bates, K. Delaney, G. Fredrickson, *Science* **336**, 434–440
255 (2012)
- 256 2. N.A. Lynd, A.J. Meuler, M.A. Hillmyer, *Prog. Polym. Sci.* **33**, 875–893 (2008)
- 257 3. M. Matsen, *Macromolecules* **45**, 2161–2165 (2012)
- 258 4. M. Huggins, *J. Chem. Phys.* **9**(5), 440 (1941)
- 259 5. P. Flory, *J. Chem. Phys.* **10**, 51 (1942)
- 260 6. S.T. Hyde, in *Handbook of Applied Surface and Colloid Chemistry*, ed. by K. Holmberg (Wiley,
261 2001); chapter 16
- 262 7. C. Huang, H. Yu, *Polymer* **48**, 4537–4546 (2007)
- 263 8. S. Lee, M. Bluemle, F. Bates, *Science* **330**, 349–353 (2010)
- 264 9. S. Kim, K. Jeong, A. Yethiraj, M. Mahanthappa, *Proc. Natl. Acad. Sci. USA* **114**(16), 4072–
265 4077 (2017). <https://doi.org/10.1073/pnas.1701608114>
- 266 10. T. Gillard, S. Lee, F. Bates, *Proc. Natl. Acad. Sci. USA* **113**(19), 167–5172 (2016)
- 267 11. N. Hadjichristidis, H. Iatrou, M. Pitsikalis, S. Pispas, A. Avgeropoulos, *Prog. Polym. Sci.* **30**,
268 725–782 (2005)
- 269 12. F. Bates, *MRS Bull.* **30**, 525–532 (2005)
- 270 13. F. Martinez-Veracoechea, F. Escobedo, *Macromolecules* **40**, 7354–7365 (2007)
- 271 14. P. Padmanabhan, E. Martinez-Veracoechea, F. Escobedo, *Macromolecules* **49**, 5232–5243
272 (2016)

- 273 15. J.J.K. Kirkensgaard, P. Fragouli, N. Hadjichristidis, K. Mortensen, *Macromolecules* **44**(3),
274 575–582 (2011)
- 275 16. J.J.K. Kirkensgaard, *Soft Matter* **6**, 6102–6108 (2010)
- 276 17. Y. Matsushita, K. Hayashida, T. Dotera, A. Takano, J. Phys. Condens. Matter **23**, 284111 (2011)
- 277 18. T. Gemma, A. Hatano, T. Dotera, *Macromolecules* **35**, 3225–3227 (2002)
- 278 19. J.J.K. Kirkensgaard, S. Hyde, *Phys. Chem. Chem. Phys.* **11**, 2016–2022 (2009)
- 279 20. S.T. Hyde, L. de Campo, C. Oguey, *Soft Matter* **5**, 2782–2794 (2009)
- 280 21. J.J.K. Kirkensgaard, M.C. Pedersen, S.T. Hyde, *Soft Matter* **10**, 7182–7194 (2014)
- 281 22. C.-I. Huang, H.-K. Fang, C.-H. Lin, *Phys. Rev. E* **77**, 031804 (2008)
- 282 23. J.J.K. Kirkensgaard, *Phys. Rev. E* **85**, 031802 (2012)
- 283 24. K. Hayashida, A. Takano, T. Dotera, Y. Matsushita, *Macromolecules* **41**, 6269–6271 (2008)
- 284 25. S. Hyde, G. Schröder, *Curr. Opin. Colloid Interface Sci.* **8** (2003),
- 285 26. Y. Han, D. Zhang, L. Chng, J. Sun, L. Zhao, X. Zou, J. Ying, *Nat. Chem.* **1**, 123–127 (2009)
- 286 27. G. Sorenson, A. Schmitt, M. Mahanthappa, *Soft Matter* **10**, 8229–8235 (2014)
- 287 28. M. Fischer, L. de Campo, J. Kirkensgaard, S. Hyde, G. Schröder-Turk, *Macromolecules* **47**,
288 7424–7430 (2014)
- 289 29. V. Abetz, S. Jiang, *e-Polymers* **054**, 1–9 (2004)
- 290 30. J. Kirkensgaard, M. Evans, L. de Campo, S. Hyde, *Proc. Natl. Acad. Sci. USA* **111**(4), 1271–
291 1276 (2014)
- 292 31. L. Carlucci, G. Ciani, D. Proserpio, *Coord. Chem. Rev.* 247–289 (2003)
- 293 32. T. Dotera, *Phys. Rev. Lett.* **82**(1), 105 (1999)
- 294 33. T. Higashihara, T. Sakurai, A. Hirao, *Macromolecules* **42**, 6006–6014 (2009)